Magnetic Resonance Imaging 58 (2019) 18–23

Contents lists available at ScienceDirect

Magnetic Resonance Imaging

journal homepage: www.elsevier.com/locate/mri

Technical note

Quantification of pathophysiological alterations in venous oxygen saturation: A comparison of global MR susceptometry techniques

Paula L. Croal[a,b], Jackie Leung[a], Charly L. Phillips[a,c], Malambing G. Serafin[a], Andrea Kassner[a,d,*]

[a] Department of Physiology and Experimental Medicine, The Hospital for Sick Children, Toronto, Ontario, Canada
[b] Institute of Biomedical Engineering, The University of Oxford, Oxford, United Kingdom
[c] Department of Systems Design Engineering, University of Waterloo, Waterloo, Ontario, Canada
[d] Department of Medical Imaging, University of Toronto, Toronto, Ontario, Canada

ARTICLE INFO

Keywords:
Venous oxygenation
Susceptibility weighted imaging
Susceptometry
Phase
Sickle cell disease
Quantitative MRI

ABSTRACT

The purpose of this study was to compare the Infinite Cylinder and Forward Field methods of quantifying global venous oxygen saturation (Y_v) in the superior sagittal sinus (SSS) from MRI phase data, and assess their applicability in systemic cerebrovascular disease.15 children with sickle cell disease (SCD) and 10 healthy age-matched controls were imaged on a 3.0 T MRI system. Anatomical and phase data around the superior sagittal sinus were acquired from a clinically available susceptibility weighted imaging sequence and converted to Y_v using the Infinite Cylinder and Forward Field methods. Y_v was significantly higher when calculated using the Infinite Cylinder method compared to the Forward Field method in both patients ($p = 0.003$) and controls ($p < 0.001$). A significant difference in Y_v was observed between patients and controls for the Forward Field method only ($p = 0.006$). While various implementations of Y_v quantification can be used in practice, the results can differ significantly. Simplistic models such as the Infinite Cylinder method may be easier to implement, but their dependence on broad assumptions can lead to an overestimation of Y_v, and may reduce the sensitivity to pathophysiological changes in Y_v.

1. Introduction

Global venous oxygen saturation (Y_v) is a clinical parameter for interpreting cerebral physiology, and is directly linked to the quantification of oxygen extraction fraction and the cerebral metabolic rate of oxygen [1]. MRI offers various methods that are capable of non-invasive Y_v quantification, both regional and global. However, global measures are currently more practical for clinical protocols due to restrictions on image acquisition times, in addition to increased robustness [2]. Of particular interest are global susceptometry methods, as they enable rapid Y_v quantification using data that can be acquired from clinically available sequences.

MR susceptometry techniques utilize the measured signal phase shift between intravascular blood and the surrounding tissue to calculate global Y_v. This difference in phase is dependent on the intravascular susceptibility, which is driven by the concentration of deoxyhemoglobin and is also a function of the vessel geometry relative to the main magnetic field. The most commonly used modeling technique for Y_v quantification from susceptibility shift is based on the *Infinite Cylinder* approximation [3–5]. This approach is favoured for its simplicity, as it assumes the vessel of interest can be described by a straight cylinder with length far greater than diameter. Whilst previously validated in large vessels such as the superior sagittal sinus (SSS) [6], it has recently been suggested that this model is not an appropriate representation of the actual vessel shape and orientation [7]. To address this potential oversimplification, Driver et al. [7] recently proposed an alternative to the *Infinite Cylinder* approach. The application of the *Forward Field* calculation [8] enables the numerical computation of the magnetic field perturbation arising from an arbitrary vessel shape such as the volume of the SSS. This technique removes the assumptions enforced by the *Infinite Cylinder* approximation and thus produces a more accurate quantification of Y_v. Preliminary results in healthy adult subjects showed that Y_v is consistently higher when measured with the *Infinite Cylinder* in comparison to the *Forward Field* approach, suggestive of systemic bias, making its validity for application in clinical studies uncertain. However, in the absence of a direct comparison of these two methods in a clinical population, their respective abilities to detect pathophysiological changes in Y_v are not known.

Here, we implement and compare the *Infinite Cylinder* and *Forward*

* Corresponding author at: Peter Gilgan Centre for Research and Learning, 8th floor, Room 08.9715, 686 Bay St, Toronto, ON M5G 0A4, Canada.
E-mail address: andrea.kassner@utoronto.ca (A. Kassner).

https://doi.org/10.1016/j.mri.2019.01.008
Received 8 September 2018; Received in revised form 9 January 2019; Accepted 10 January 2019

Field methods for Y_v quantification in a clinical population suffering from systemic cerebrovascular disease and at high risk of ischemic damage, specifically children with sickle cell disease (SCD). Paediatric SCD is characterised by chronic hemolytic anemia and microvascular occlusion, which alters oxygen dynamics in the brain [9] and puts patients at increased risk of severe neurological complications such as overt ischemic stroke, silent cerebral infarcts and neurocognitive morbidity [10]. The primary hypothesis is that due to more detailed modeling of vessel shape and orientation, the *Forward Field* approach will provide a quantifiable improvement in the detection of pathophysiological changes in Y_v. A secondary hypothesis is that Y_v quantified with the *Forward Field* approach will be more strongly associated with markers of disease severity in patients with SCD, than with the *Infinite Cylinder* method.

2. Materials and methods

2.1. Subject recruitment

The study was approved by our institutional Research Ethics Board and informed written consent was obtained from all subjects prior to the study, conforming to the standards of the Declaration of Helsinki for medical research involving human subjects. Fifteen children (14.4 ± 2.4 years, 9 male, 6 female) with sickle cell disease (14 HbSS, 1 HbSβ^+) were recruited from our institution's Haematology clinic and included in this study. Exclusion criteria included a history of focal neurologic events lasting > 24 h or blood transfusion therapy (chronic or emergent) within 3 months of the study. For comparison, ten healthy age-matched children (13.6 ± 3.7 years, 6 male, 4 female) were included. All subjects were asked to abstain from consuming caffeinated and/or alcoholic beverages on the day of the MR scan.

2.2. MRI protocol

Image acquisition was performed on a 3.0 Tesla clinical MRI scanner (Magnetom Tim Trio, Siemens Medical Solutions, Erlangen, Germany) using a 32-channel head coil. For Y_v quantification, magnitude and phase data were acquired using a 3D FLASH sequence available via a clinically available flow-compensated susceptibility-weighted imaging (SWI) package (TR/TE = 28/20 ms; FA = 15°; voxel size = 0.85 × 0.7 × 1.2 mm; slices = 72; FOV = 230 × 172 mm; acceleration factor = 2; duration = 5 min). The slices were prescribed orthogonal to the main magnetic field (B_0) with the lowest slice including the confluence of sinuses. Phase images were homodyne filtered as part of Siemen's online SWI post-processing using a Hanning window size of 64 × 64 [11,12].

Pulsed arterial spin-labeling (ASL) data were acquired using a clinically available sequence (2D-EPI PICORE Q2TIPS: TI_1 = 700 ms, TI_2 = 1800 ms) [13]. A total of 91 dynamics were acquired, consisting of a proton-density calibration (M_0) image followed by 45 tag-control image pairs. The cerebral blood flow (CBF) quantification pipeline with PASL has been previously described in detail [14]; in brief subtracted perfusion-weighed pairs were fit to a single-compartment kinetic model [15] on a voxelwise basis, assuming T_1 of arterial blood of 1818 ms for patients [16], and 1650 ms for controls [17]. High-resolution T_1-weighted anatomical images were acquired using a 3D MPRAGE sequence (TR/TE = 2300/2.96 ms, FOV = 256 mm, 1.0 mm isotropic resolution) for isolation of grey matter (GM) CBF, following nonlinear registration between images (FNIRT, FSL).

2.3. Haematologic measures

For patients, measures of haematocrit (*Hct*) were recorded from a complete blood count acquired from a clinical blood draw taken within 30 days of the MRI scan. For healthy volunteers, *Hct* values were assumed to be 0.41 for males and 0.39 for females, based on literature values [18].

2.4. Y_v quantification

Global Y_v was calculated according to Eq. (1) by considering the measured phase shift in the vicinity of the superior sagittal sinus (SSS):

$$Y_v = 1 - \frac{\Delta\varphi_{IV}}{A{\cdot}\gamma{\cdot}TE{\cdot}B_0{\cdot}Hct{\cdot}\Delta\chi_{do}}, \quad (1)$$

where γ is the proton gyromagnetic ratio ($\gamma = 2.675 \times 10^8\,\mathrm{rad{\cdot}s^{-1}{\cdot}T^{-1}}$), TE is echo time, B_0 is field strength, *Hct* is haematocrit and $\Delta\chi_{do}$ is the volume susceptibility difference between fully deoxygenated and oxygenated hemoglobin ($\Delta\chi_{do}$ = 0.27 ppm). $\Delta\phi_{IV}$ is the difference between the mean phase measured within the SSS and the mean phase of the surrounding tissue, and A is a geometric parameter representing the contribution to the magnetic field distortion caused by the shape and orientation of the vessel. Both $\Delta\phi_{IV}$ and A parameters are subject specific and are estimated from the MRI data. Image post-processing and simulations were performed using in-house code (MATLAB version 2013b, The MathWorks Inc., Natick, MA).

2.4.1. Infinite cylinder method

By modeling the SSS as a sufficiently long and uniform cylinder, the geometric term A can be simplified to a closed form solution:

$$A = \frac{(3\cos^2\theta - 1)}{6}, \quad (2)$$

where θ represents the angle between the longitudinal axis of the cylinder and the main magnetic field B_0, which was measured in the sagittal plane for each subject (Fig. 1) using the Mango Multi-image analysis GUI (http://rii.uthscsa.edu/mango/).

The phase difference ($\Delta\phi_{IV}$) from Eq. (1) corresponding to this model was calculated by defining appropriate regions of interest (ROI) in slices representative of this cylinder orientation. First, a ROI of the SSS was manually drawn on the SWI magnitude image on five contiguous slices in which the SSS was most straight. To minimize potential confounds from partial volume effects, an intravascular ROI (ROI_{IV}) was formed by eroding the SSS ROI inward by one voxel. An extravascular ROI (ROI_{EV}) was defined for the surrounding tissue by dilating the sagittal sinus ROI by seven voxels and then removing the center of the ROI, leaving a two voxel wide region surrounding the SSS for each slice. ROIs were subsequently applied to the filtered phase image (Fig. 1), and intensity-based thresholding applied to the ROI_{EV} to remove any residual extravascular contributions from smaller vessels (consistent across all subjects). Mean intravascular and extravascular phase were calculated, and resulting phase difference values used to calculate Y_v for each slice, all of which were averaged to determine per subject measures.

2.4.2. Forward field method

In the absence of any assumptions about the geometry and orientation of the SSS, the parameter A can only be estimated through numerical methods. Similar to the *Infinite Cylinder* method, an ROI for the SSS was defined from the SWI magnitude image, but extended to include all slices where a clear cross-section of the vein was visible. Subsequently, ROI_{IV} and ROI_{EV} were defined across these slices by erosion and dilation, as described earlier.

A was found using the *Forward Field* calculation [8]. Briefly, the manually drawn ROI volume representing the SSS was incorporated into a numerical simulation in which the vessel shape was assigned an arbitrary susceptibility value of 1 unit and the surrounding uniform medium was assigned a susceptibility value of 0 units. Next, the susceptibility map was padded to centre the SSS ROI in a cubic matrix of uniform dimensions. The relative perturbation of the magnetic field pattern was then simulated for this geometric configuration by convolving the susceptibility map with the unit dipole field or convolution

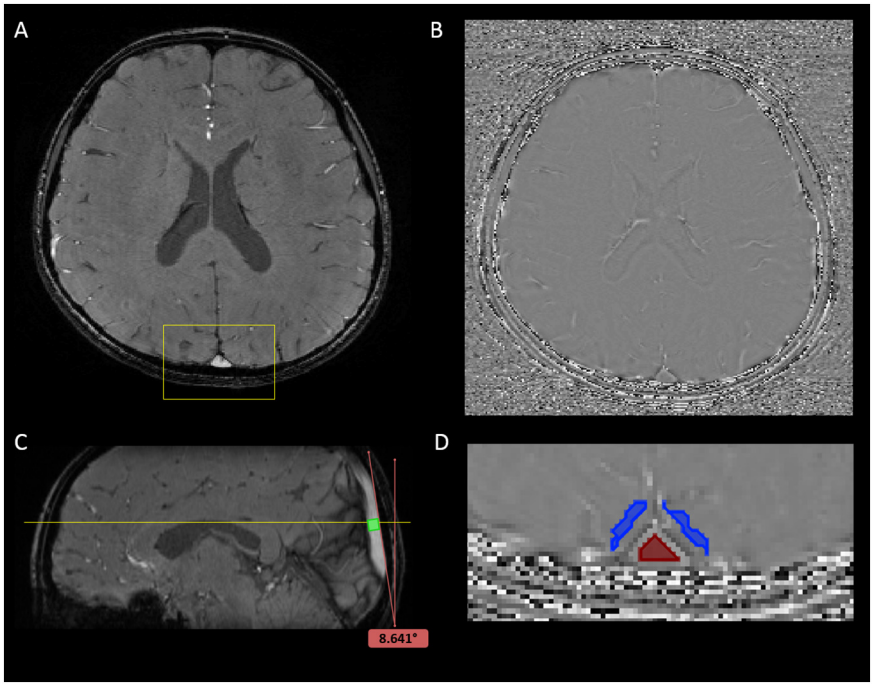

Fig. 1. Example of region of interest (ROI) selection in the susceptibility-weighted image (SWI) of a representative control subject. The superior sagittal sinus (SSS) can be visualised on an axial slice of the magnitude (A) and phase (B) images. (C) The location of the selected slice in the sagittal view is signified by the yellow line, with angle from B_0 shown in pink. The green region indicates the 5 contiguous slices used for the Infinite Cylinder approximation. (D) Automated segmentation and erosion/dilation generates the intravascular (red) and extravascular (blue) ROIs, which are overlaid onto the phase image. (For interpretation of the references to colour in this figure legend, the reader is referred to the web version of this article.)

kernel, presented as Eq. (4) of Wharton et al., in order to orient the magnetic field perpendicular to the image slices [19]. This simulation was performed in the Fourier domain and took into account the anisotropic voxel dimensions of the image data (MATLAB version 2013b, The MathWorks Inc., Natick, MA). Inverse 3D discrete fast Fourier transform was carried out, and the resulting field perturbation map was unpadded in order to align with the original image. *A* was calculated as the difference between the average field perturbation in the ROI_{IV} and ROI_{EV} at each image slice. $\Delta\phi_{IV}$ was also calculated for each pair of ROIs, such that A, $\Delta\phi_{IV}$, and subsequently Yv, were available for each subject on a slice-by-slice basis. Upper and lower slices were discarded due to edge effects, and parameters averaged across remaining slices to obtain mean values to be used for subsequent analysis.

The SSS diameter was manually measured, and subsequently averaged, across all slices selected for analysis, using the 'Ruler' tool in the Mango Multi-Image Analysis GUI (http://ric.uthscsa.edu/mango/download.html).

2.5. Statistical analysis

Between-group statistical comparisons were made using a two-tailed Welch's *t*-test, and within-group comparisons were made using a two-tailed paired Student's *t*-test. Correlations between Y_v quantified with the *Forward Field* and *Infinite Cylinder* methods, and Y_v with both *Hct* and GM CBF, were assessed separately in patients and controls using the Pearson product-moment correlation coefficient. Statistical tests were implemented in *R* [20], and $p < 0.05$ were considered significant.

3. Results

All subjects completed the scan session as planned. Manual inspection of EV and IV ROIs showed residual IV contributions in the EV ROI, and so the EV ROI was re-made by dilating the SSS ROI by nine voxels, rather than 7.

Haematologic parameters are summarised in Table 1, and overview of MRI-based parameters used for Y_v quantification given in Table 2. Method choice had no significant impact on $\Delta\phi_{IV}$ in either patients or controls ($p = 0.083$ and $p = 0.32$ respectively). However,

Table 1
Subject characteristics and haematologic variables (mean ± SD).

Variable	Healthy controls	Patients with SCD
Age (years)	13.6 ± 3.7	14.5 ± 2.4
Sex (M/F)	6/4	9/6
Haematocrit	–	0.288 ± 0.028
Hemoglobin (g/dL)	–	101.3 ± 10.1
Reticulocytes (%)	–	7.48 ± 3.23
Absolute Reticulocytes (K/mm^3)	–	225.8 ± 86.4
Mean corpuscular volume (fL)	–	95.2 ± 12.6
SaO_2 (%)	–	99.0 ± 0.02
White Blood Cells ($\times 10^9$/L)	–	10.2 ± 4.0
Neutrophils ($\times 10^9$/L)	–	5.66 ± 3.99
Lymphocytes ($\times 10^9$/L)	–	3.15 ± 0.82
Platelets ($\times 10^9$/L)	–	371.1 ± 131.6

Table 2
Quantification of venous oxygen saturation for patients with sickle cell disease and healthy controls.

	Healthy controls	Patients with SCD	*p*-Value
Hct	0.402 ± 0.1	0.289 ± 0.26	–
GM CBF (ml/min/100 g)	32.8 ± 14.5	59.1 ± 11.9	< 0.001
A_{IC}	0.298 ± 0.025	0.291 ± 0.028	0.51
A_{FF}	0.227 ± 0.022	0.207 ± 0.03	0.062
$\Delta\phi_{IV\_IC}$	0.113 ± 0.042	0.0704 ± 0.028	0.014
$\Delta\phi_{IV\_FF}$	0.121 ± 0.024	0.0591 ± 0.018	< 0.001
Y_{vIC}	0.772 ± 0.067	0.805 ± 0.074	0.26
Y_{vFF}	0.692 ± 0.049	0.758 ± 0.057	0.006
Number of $Slices_{IC}$	5	5	–
Number of $Slices_{FF}$	26 ± 6	21 ± 8	0.112
Θ_{IC} (°)	14.3 ± 5.7	16.1 ± 6.6	0.52
SSS Diameter (mm)	7.8 ± 1.4	8.9 ± 1.4	0.07

GM CBF, Grey matter cerebral blood flow, *A*, geometric parameter; $\Delta\phi_{IV}$, measured change in intravascular-extravascular phase; Y_v, venous oxygen saturation; SCD, sickle cell disease. IC and FF subscripts denote Infinite Cylinder and Forward Field methods, respectively. Data presented as group averages ± SD.

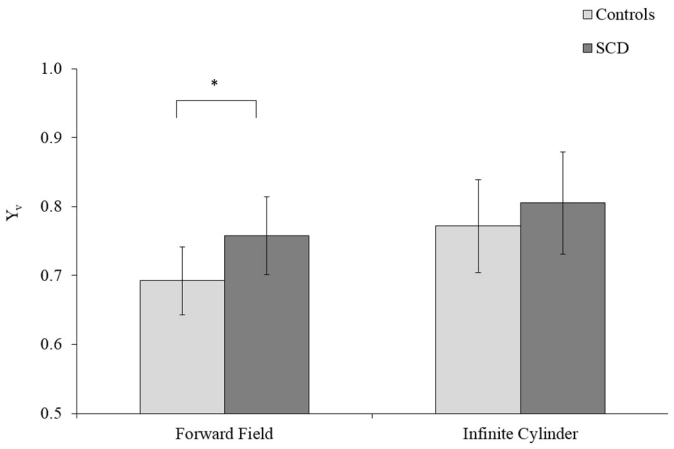

Fig. 2. A significant elevation in venous oxygen saturation (Y_v) was observed in children with sickle cell disease (SCD) as measured with the Forward Field method in comparison to healthy controls ($p = 0.006$). No significant difference was observed between patients and controls with the Infinite Cylinder method ($p = 0.26$).

quantification of A using the *Forward Field* method gave values significantly lower than for the *Infinite Cylinder* method ($p < 0.001$ for both patients and controls). For both patients and controls, Y_v measured with the *Infinite Cylinder* method was significantly higher than it was when measured with the *Forward Field* method ($p = 0.003$ and $p < 0.001$ for patients and controls respectively). GM CBF was significantly elevated in patients in comparison to healthy controls (Table 2, $p < 0.001$). Mean variance in Y_v across slices was 0.022 in patients and 0.019 in controls as measured with the *Forward Field* method. For the *Infinite Cylinder* method, mean variance in Y_v across slices was 0.003 in patients and 0.006 in controls. This through-plane variance in Y_v did not differ significantly between patients and controls for either method.

Patients with SCD showed a significant reduction in $\Delta\phi_{IV}$ in comparison to controls for both methods ($p = 0.014$ and $p < 0.001$ for *Infinite Cylinder* and *Forward Field* methods respectively), while there were no significant between-group differences in measurements of A. For the *Forward Field* method, this led to a significant elevation in Y_v in patients with SCD (Fig. 2, $p = 0.006$). There were no significant differences in Y_v in SCD patients when the *Infinite Cylinder* method was used (Fig. 2, $p = 0.26$). No significant differences in SSS diameter were observed ($p = 0.07$).

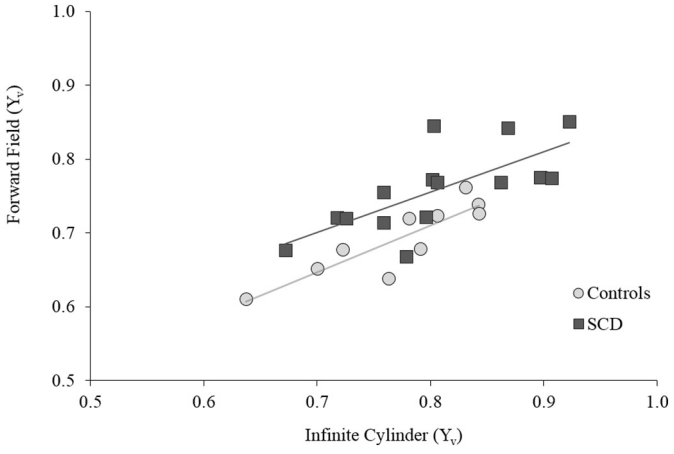

Fig. 3. A significant positive correlation was observed in venous oxygen saturation (Y_v) as measured with the Forward Field and Infinite Cylinder method in both healthy controls ($r = 0.88$, $p < 0.001$) and patients with sickle cell disease (SCD) ($r = 0.71$, $p = 0.003$).

Correlation analysis between Y_v quantified using the *Forward Field* method and the *Infinite Cylinder* method (Fig. 3) revealed a strong positive correlation for both healthy controls ($r = 0.88$, $p < 0.001$), and patients with SCD ($r = 0.71$, $p = 0.003$). Correlation analysis between Y_v with *Hct* in patients with SCD (Fig. 4A) revealed a strong negative association for both the *Infinite Cylinder* method ($r = -0.64$, $p = 0.046$), and *Forward Field* method ($r = -0.60$, $p = 0.018$). *Hct* was assumed for healthy controls, thus correlation with Y_v was not assessed. Correlation analysis between Y_v with GM CBF (Fig. 4B) revealed a significant negative association for patients with SCD for the *Forward Field* ($r = -0.66$, $p = 0.007$) and a trend for the *Infinite Cylinder* method, which did not reach statistical significance ($r = -0.52$, $p = 0.12$). No significant association was observed between Y_v and GM CBF in healthy controls for either the *Infinite Cylinder or Forward Field* method.

4. Discussion

The present study demonstrates the application of two clinically feasible MR susceptometry techniques for measuring global Y_v in patients with cerebrovascular disease. Importantly, we highlight the limitations of using the *Infinite Cylinder* model in comparison to the more recent *Forward Field* method when assessing a clinical population, at the potential cost of more demanding acquisition (pre-requisite of 3D field map, with associated time penalty) and computational load. Only for the *Forward Method* was a significant increase in Y_v observed in patients with SCD in comparison to healthy controls, in line with findings of a recent TRUST MRI study, optimised for application in SCD patients [9]. However, earlier TRUST MRI studies have reported a conflicting reduction in Y_v in patients with SCD [21,22], however this plausibly reflects inappropriate calibration method in this disease population, rather than actual pathological changes [9].

Previous research comparing quantification strategies in healthy volunteers reported similar within-group results [7]. Modeling the SSS as a long and uniform cylinder parallel to B_0 assumes the maximal value for the geometric parameter A and will ultimately lead to an overestimation of Y_v compared to other analysis methods. Nonetheless, the *Infinite Cylinder* model has previously been considered an appropriate strategy in clinical studies on brain injury [23,24]. However, in a group of patients with traumatic brain injury, Ragan et al. report the need to exclude those with moderate disease severity due to wide variability in measured values [23]. It was not possible for the authors to distinguish methodological error from disease variability, highlighting the need for a global quantification method to better account for individual variability associated with vessel geometry and orientation. In an effort to maximise the accuracy of the *Infinite Cylinder* method, we relaxed the common assumption that the SSS is perpendicular to B0, thus also the assumptions that such $\Theta = 0^{\circ}$, and $A = 1/3$. Instead, Θ was measured on an individual basis, slightly increasing the complexity of this approach, but not dramatically so. Nonetheless, Y_v remained significantly higher in comparison to the *Forward Field* approach, in line with the more simplistic implementation of the *Infinite Cylinder* [25]. Without a gold standard for comparison, it is difficult to objectively ascertain whether Y_v is truly overestimated with the *Infinite Cylinder* approach; whilst both analysis methods produce Y_v values within the physiologically plausible range of 60–80% [26], the *Forward Field* method is more in line with the reported range (63–73%) in previous MRI studies of healthy volunteers [4,5,27–29].

Both methods compared in this study are based on susceptometry principles, which assume a fixed susceptibility difference between blood and tissue ($\Delta\chi_{do}$). Recent in-vitro research has indicated potential susceptibility changes in the red blood cells of SCD patients [30], but the overall impact on the quantification has not yet been verified. In addition, blood samples were not collected from healthy volunteers, thus *Hct* values were estimated based on known literature values. These assumptions, however, were common to both methods, and as such are

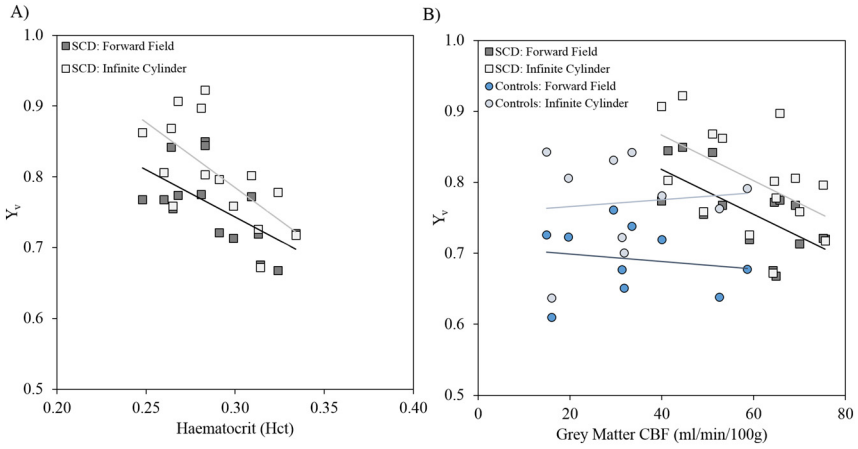

Fig. 4. . A) A significant negative correlation was observed between haematocrit (Hct) and venous oxygen saturation (Y_v) in patients with SCD, as measured with both the Forward Field ($r = -0.60$, $p = 0.018$) and Infinite Cylinder ($r = -0.64$, $p = 0.046$) method. B) A significant negative correlation was observed between grey matter cerebral blood flow (CBF) and Yv in patients with SCD for the Forward Field method ($r = -0.66$, $p = 0.007$), while a similar trend was observed for the Infinite Cylinder method ($r = -0.52$, $p = 0.12$). No association was observed between grey matter CBF and Y_v in control subjects.

unlikely to significantly bias the comparison. Due to the anaemic nature of the disease, it is highly likely that the variability in *Hct* is greater for patients with SCD than for healthy controls, which may contribute to the increased variability in Y_v in patients in comparison to controls, for both analysis methods.

In addition to the two methods presented here, a wide range of alternative MRI techniques for both global and regional Y_v quantification have been developed [29,31–33]. However, in terms of clinical relevance, global susceptometry methods are currently preferable as the SWI sequence is readily available on clinical scanners and the data acquisition time is appropriate for clinical practice. Furthermore, these methods do not require prior calibration to scanners, sequences, field strength or haematologic values, making them more feasible for multicentre or longitudinal trials [2].

It has been previously shown that there may be a loss of phase information if the Hanning window size is too large for the vessel of interest [34]. Here, a window size of 64 × 64 was utilised, as filtering was performed as part of Siemen's standard on-line processing of SWI data [12]. Given the measured diameter of the SSS, the use of this window size may have led to an overestimation in Y_v for both the *Forward Field* and *Infinite Cylinder* methods. This was observed in Driver et al.'s intravascular measurements of Y_v in healthy volunteers, particularly when the *Infinite Cylinder* method was applied [7]. However, no significant differences in the SSS diameter were observed between patients and controls. Thus, while absolute Y_v may have been impacted, any between-group differences should remain unaffected.

While a significant correlation between *Infinite Cylinder* and *Forward Field* measures of Y_v was observed for both patients and controls, the association was considerably stronger for controls. The weaker correlation in patients highlights the importance of performing validation in a clinical population. Our results suggest that accurate modeling of the entire vessel shape may be necessary for reliable clinical evaluation of Y_v, particularly in patients with known vasculopathy. Furthermore, for both subject groups, a lower coefficient of variation is observed for the *Forward Field* method, nonetheless, a reproducibility study is warranted to assess potential differences in robustness between the two methods. In patients with SCD, correlation analysis between Y_v and GM CBF revealed a significant inverse association for the *Forward Field* method only, with oxygenation reducing as CBF increases. This trend was also observed for the *Infinite Cylinder* method, but did not reach significance, further supporting the notion that the *Forward Field* method is more sensitive to pathological alterations. No association was observed in healthy controls, for either method. This relationship has not previously been assessed in a paediatric SCD population, but is in contrast to previous reports in adults with SCD, where both no association, and positive associations have been reported, depending on patient grouping [21,35]. Such differences could arise from both technical and/or physiological sources. Firstly, Bush et al., [35], with whom our results most closely align, implemented phase-contrast MRI measures of total brain blood flow, whereas we measure tissue-level perfusion. It has previously been established that bulk flow may not be indicative of tissue-level perfusion in SCD [36], thus direct comparison is challenging. Secondly, patient demographics differed significantly between this study and previous work, where adults (including those undergoing transfusion therapy) were imaged. Adult and paediatric physiology and pathophysiology, and degree of impairment, likely differ in SCD [10,37], as such our results may reflect more intact haemodynamic compensatory mechanisms in children with SCD. Thirdly, the majority of patients in this study (10/15) were undergoing treatment with hydroxyurea, which is known to manipulate CBF. While this makes physiological interpretation more challenging, it accurately reflects current demographics in paediatric patients with SCD.

It is likely that our reported CBF values are slightly underestimated in this specific patient group, given the range of technical challenges in both acquisition and analysis of ASL in SCD [38–40]. We have previously discussed the challenges posed by our current ASL implementation [36], and given recent findings, agree with recent SCD-specific recommendations that future ASL studies in this population should ideally implement multiple post-label delays, such that arterial transit time can be quantified and kinetic modeling expanded to a two-compartment model [40,41]. Furthermore, a pseudo-continuous rather than pulsed labeling scheme would likely maximise inversion efficiency in this high flow environment [35,38,42]. Despite these technical limitations, given that CBF has been reported in this study to allow for correlation analysis against the Infinite Cylinder and Forward Field measures of Y_v, our conclusions are unlikely to be significantly impacted.

A significant inverse association between *Hct* and Y_v exists for both analysis methods, interestingly, the association was marginally stronger for the *Infinite Cylinder* method, which could be attributed to the larger range in Y_v in the *Infinite Cylinder* approach (0.67–0.85 for *Forward Field*, and 0.67–0.92 for *Infinite Cylinder*) [43]. Nonetheless, it appears that both approaches show reasonable agreement with *Hct*, with increased venous oxygenation with increasing anemia, in line with the recent findings of Bush et al. [44] with *HbS* specific calibrated TRUST MRI, but in contrast to findings using the standard TRUST MRI calibration method [21,44]. While TRUST MRI is often posited as the most feasible method for quantification of venous oxygenation, findings in patients with SCD are significantly impacted by choice of calibration model. This is problematic in a patient group where an array of between-group differences may already arise due to age, clinical history, and therapeutic intervention. Thus, the correlations we observe between Y_v and *Hct*, in this study provide further support for the HbS calibration model in TRUST MRI. However, further comparisons with TRUST MRI are warranted, within the same patients.

5. Conclusions

In conclusion, the results presented in this study reveal the benefits of adopting the *Forward Field* analysis method for measuring Y_v using MRI. Our findings are not limited to global quantification strategies, as the *Infinite Cylinder* approximation has previously been implemented in regional analysis around smaller veins [24]. By further developing these techniques, rapid and reliable assessment of oxygen delivery and consumption will become clinically feasible, providing valuable insight into the mechanisms associated with cerebral metabolic dysfunction.

Acknowledgements

This work was funded by Canadian Institutes of Health Research (CIHR) and Canada Research Chairs (CRC). We wish to thank Dr. Suzan Williams for patient recruitment, Dr. Ian Driver for helpful discussions relating to the implementation of the Forward Field method, and Tammy Rayner and Ruth Weiss for operating the MR scanner. Our appreciation also goes to all the participants who volunteered their time for this study.

Grant support

This work was supported by the Canadian Institutes of Health Research [grant number 1111113]; and Canada Research Chairs [grant number 72029767]. The funding sources had no involvement in the study design; in the collection, analysis and interpretation of data; in the writing of the report; and in the decision to submit the article for publication.

References

[1] Kety SS, Schmidt CF. The effects of altered arterial tensions of carbon dioxide and oxygen on cerebral blood flow and cerebral oxygen consumption of Normal Young men. J Clin Invest 1948;27:484–92.
[2] Rodgers ZB, Englund EK, Langham MC, Magland JF, Wehrli FW. Rapid T2- and susceptometry-based CMRO2 quantification with interleaved TRUST (iTRUST). NeuroImage 2015;106:441–50.
[3] Haacke EM, Lai S, Reichenbach JR, Kuppusamy K, Hoogenraad FG, Takeichi H, et al. In vivo measurement of blood oxygen saturation using magnetic resonance imaging: a direct validation of the blood oxygen level-dependent concept in functional brain imaging. Hum Brain Mapp 1997;5:341–6.
[4] Fernández-Seara M, Techawiboonwong A, J a Detre, Wehrli FW. MR susceptometry for measuring global brain oxygen extraction. Magn Reson Med 2006;55:967–73.
[5] Jain V, Langham MC, Wehrli FW. MRI estimation of global brain oxygen consumption rate. J Cereb Blood Flow Metab 2010;30:1598–607.
[6] Li C, Langham MC, Epstein CL, Magland JF, Wu J, Gee J, et al. Accuracy of the cylinder approximation for susceptometric measurement of intravascular oxygen saturation. Magn Reson Med 2012;67:808–13.
[7] Driver ID, Wharton SJ, Croal PL, Bowtell R, Francis ST, Gowland PA. Global intravascular and local hyperoxia contrast phase-based blood oxygenation measurements. NeuroImage 2014;101:458–65.
[8] Marques JP, Bowtell R. Application of a Fourier-based method for rapid calculation of field inhomogeneity due to spatial variation of magnetic susceptibility. Concepts Magn Reson Part B: Magn Reson Eng 2005;25B:65–78.
[9] Bush AM, Coates TD, Wood JC. Diminished cerebral oxygen extraction and metabolic rate in sickle cell disease using T2 relaxation under spin tagging MRI. Magn Reson Med 2018;80:294–303.
[10] Ohene-Frempong K, Weiner SJ, Sleeper LA, Miller ST, Embury S, Moohr JW, et al. Cerebrovascular accidents in sickle cell disease: rates and risk factors. Blood 1998;91:288–94.
[11] Noll DC, Nishimura DG, Macovski A, Detection A. Homodyne detection in magnetic resonance imaging. IEEE Trans Med Imaging 1991;I. (164–163).
[12] Haacke EM, Mittal S, Wu Z, Neelavalli J, Cheng Y-CN. Susceptibility-weighted imaging: technical aspects and clinical applications, part 1. AJNR Am J Neuroradiol 2009;30:19–30.
[13] Luh WM, Wong EC, Bandettini PA, Hyde JS. QUIPSS II with thin-slice TI1 periodic saturation: a method for improving accuracy of quantitative perfusion imaging using pulsed arterial spin labeling. Magn Reson Med 1999;41:1246–54.
[14] Croal PL, Leung J, Kosinski PD, Shroff M, Odame I, Kassner A. Assessment of cerebral blood flow with magnetic resonance imaging in children with sickle cell disease: a quantitative … assessment of cerebral blood flow with magnetic resonance imaging in children with sickle cell disease: a quantitative comparison. Brain Behav 2017;7:e00811.
[15] Wong EC, Buxton RB, Frank LR. Quantitative imaging of perfusion using a single subtraction (QUIPSS and QUIPSS II). Magn Reson Med 1998;39:702–8.
[16] Vaclavu L, van der Land V, Heijtel DFR, van Osch MJP, Cnossen MH, Majoie CBLM, et al. In vivo T1 of blood measurements in children with sickle cell disease improve cerebral blood flow quantification from arterial spin-labeling MRI. Am J Neuroradiol 2016;37:1727–32.
[17] Alsop DC, Detre JA, Golay X, Günther M, Hendrikse J, Hernandez-Garcia L, et al. Recommended implementation of arterial spin-labeled perfusion MRI for clinical applications: a consensus of the ISMRM perfusion study group and the European consortium for ASL in dementia. Magn Reson Med 2015;73:102–16.
[18] Daniel WA. Hematocrit: maturity relationship in adolescence. Pediatrics 1973;52:388–94.
[19] Wharton S, Schäfer A, Bowtell R. Susceptibility mapping in the human brain using threshold-based k-space division. Magn Reson Med 2010;63:1292–304.
[20] Development Core R, Team RFFSC. R: a language and environment for statistical computing. Vienna Austria R Found Stat Comput. 1. 2008. (ISBN 3-900051-07-0).
[21] Jordan LC, Gindville MC, Scott AO, Juttukonda MR, Strother MK, Kassim AA, et al. Non-invasive imaging of oxygen extraction fraction in adults with sickle cell anaemia. Brain 2016. https://doi.org/10.1093/brain/awv397.
[22] Watchmaker JM, Juttukonda MR, Davis LT, Scott AO, Faraco CC, Gindville MC, et al. Hemodynamic mechanisms underlying elevated oxygen extraction fraction (OEF) in moyamoya and sickle cell anemia patients. J Cereb Blood Flow Metab 2018;38:1618–30.
[23] Ragan DK, McKinstry R, Benzinger T, Leonard J, Pineda J a. Depression of whole-brain oxygen extraction fraction is associated with poor outcome in pediatric traumatic brain injury. Pediatr Res 2012;71:199–204.
[24] Li M, Hu J, Miao Y, Shen H, Tao D, Yang Z, et al. In vivo measurement of oxygenation changes after stroke using susceptibility weighted imaging filtered phase data. PLoS One 2013;8:1–6.
[25] Driver I, Wharton SJ, Croal PL, Bowtell R, Francis S, Gowland P. Global intravascular and local hyperoxia contrast phase-based blood oxygenation measurements. Proc Int Soc Magn Reson Med 2013;21.
[26] Lough M, Thompson C. Urden L, editor. Critical care nursing. Mosby; 2014.
[27] Xu F, Ge Y, Lu H. Non-invasive quantification of whole-brain cerebral metabolic rate of oxygen by MRI. Magn Reson Med 2009;62:141–8.
[28] Barhoum S, Rodgers ZB, Langham M, Magland JF, Li C, Wehrli FW. Comparison of MRI methods for measuring whole-brain venous oxygen saturation. Magn Reson Med 2015;2128:2122–8.
[29] Bolar DS, Rosen BR, Sorensen AG, Adalsteinsson E. QUantitative Imaging of eXtraction of oxygen and TIssue consumption (QUIXOTIC) using venular-targeted velocity-selective spin labeling. Magn Reson Med 2011;66:1550–62.
[30] Sakhnini L, Khuzaie R. Magnetic behavior of human erythrocytes at different hemoglobin states. Eur Biophys J 2001;30:467–70.
[31] Lu H, Ge Y. Quantitative evaluation of oxygenation in venous vessels using T2-relaxation-under-spin-tagging MRI. Magn Reson Med 2008;60:357–63.
[32] Fan AP, Benner T, Bolar DS, Rosen BR, Adalsteinsson E. Phase-based regional oxygen metabolism (PROM) using MRI. Magn Reson Med 2012;67:669–78.
[33] Liu P, Xu F, Lu H. Test–retest reproducibility of a rapid method to measure brain oxygen metabolism. Magn Reson Med 2013;69:675–81.
[34] Haacke EM, Reichenbach JR. Susceptibility weighted imaging in MRI: basic concepts and clinical applications. Wiley-Blackwell; 2011.
[35] Bush AM, Borzage MT, Choi S, Václavů L, Tamrazi B, Nederveen AJ, et al. Determinants of resting cerebral blood flow in sickle cell disease. Am J Hematol 2016;91:912–7.
[36] Croal PL, Leung J, Kosinski P, Shroff M, Odame I, Kassner A. Assessment of cerebral blood flow with magnetic resonance imaging in children with sickle cell disease: a quantitative comparison with transcranial Doppler ultrasonography. Brain Behav 2017;7.
[37] Kosinski PD, Croal PL, Leung J, Williams S, Odame I, Hare GMT, et al. The severity of anaemia depletes cerebrovascular dilatory reserve in children with sickle cell disease: a quantitative magnetic resonance imaging study. Br J Haematol 2017;176:280–7.
[38] Juttukonda MR, Jordan LC, Gindville MC, Davis LT, Watchmaker JM, Pruthi S, et al. Cerebral hemodynamics and pseudo-continuous arterial spin labeling considerations in adults with sickle cell anemia. NMR Biomed 2017;30:e3681.
[39] Gevers S, Nederveen AJ, Fijnvandraat K, van den Berg SM, van Ooij P, Heijtel DF, et al. Arterial spin labeling measurement of cerebral perfusion in children with sickle cell disease. J Magn Reson Imaging 2012;35:779–87.
[40] Bush A, Chai Y, Young S, Vaclavu L, Holland S, Nederveen A, et al. Pseudo continuous arterial spin labeling quantification in anemic subjects with hyperemic cerebral blood flow. Magn Reson Imaging 2018;47:137–46.
[41] Hu HH, Rusin JA, Peng R, Shao X, Smith M, Krishnamurthy R, et al. Multi-phase 3D arterial spin labeling brain MRI in assessing cerebral blood perfusion and arterial transit times in children at 3T. Clin Imaging 2019;53:210–20.
[42] Alsop DC, J a Detre, Golay X, Günther M, Hendrikse J, Hernandez-Garcia L, et al. Recommended implementation of arterial spin-labeled perfusion MRI for clinical applications: a consensus of the ISMRM perfusion study group and the European consortium for ASL in dementia. Magn Reson Med 2014;116:102–16.
[43] Glass GV, Hopkins KD. Statistical method in education and psychology. 3rd ed. Allyn & Bacon; 1996.
[44] Bush AM, Borzage MT, Choi S, Lena V, Coates TD, Wood JC. Determinants of resting cerebral blood flowin. Am J Hematol 2016;91:912–7.